Pharmaceutical Research, Vol. 25, No. 7, July 2008 (© 2007)
DOI: 10.1007/s11095-007-9513-z

Research Paper

Cytotoxicity of Paclitaxel in Biodegradable Self-Assembled Core-Shell Poly (Lactide-Co-Glycolide Ethylene Oxide Fumarate) Nanoparticles

Xuezhong He,[1] Junyu Ma,[1] Angel E. Mercado,[1] Weijie Xu,[1] and Esmaiel Jabbari[1,2,3]

Received August 8, 2007; accepted November 30, 2007; published online January 15, 2008

Purpose. Biodegradable core-shell polymeric nanoparticles (NPs), with a hydrophobic core and hydrophilic shell, are developed for surfactant-free encapsulation and delivery of Paclitaxel to tumor cells.
Methods. Poly (lactide-co-glycolide fumarate) (PLGF) and Poly (lactide-fumarate) (PLAF) were synthesized by condensation polymerization of ultra-low molecular weight poly(L-lactide-co-glycolide) (ULMW PLGA) with fumaryl chloride (FuCl). Similarly, poly(lactide-co-ethylene oxide fumarate) (PLEOF) macromer was synthesized by reacting ultra-low molecular weight poly(L-lactide) (ULMW PLA) and PEG with FuCl. The blend PLGF/PLEOF and PLAF/PLEOF macromers were self-assembled into NPs by dialysis. The NPs were characterized with respect to particle size distribution, morphology, and loading efficiency. The physical state and miscibility of Paclitaxel in NPs were characterized by differential scanning calorimetry. Tumor cell uptake and cytotoxicity of Paclitaxel loaded NPs were measured by incubation with HCT116 human colon carcinoma cells. The distribution of NPs *in vivo* was assessed with $Apc^{Min/+}$mouse using infrared imaging.
Results. PLEOF macromer, due to its amphiphilic nature, acted as a surface active agent in the process of self-assembly which produced core-shell NPs with PLGF/PLAF and PLEOF macromers as the core and shell, respectively. The encapsulation efficiency ranged from 70 to 56% and it was independent of the macromer but decreased with increasing concentration of Paclitaxel. Most of the PLGF and PLAF NPs degraded in 15 and 28 days, respectively, which demonstrated that the release was dominated by hydrolytic degradation and erosion of the matrix. As the concentration of Paclitaxel was increased from 0 to 10, and 40 μg/ml, the viability of HCT116 cells incubated with free Paclitaxel decreased from 100 to 65 and 40%, respectively, while those encapsulated in PLGF/PLEOF NPs decreased from 93 to 54 and 28%.
Conclusions. Groups with Paclitaxel loaded NPs had higher cytotoxicity compared to Paclitaxel directly added to the media at the same concentration. NPs acted as reservoirs to protect the drug from epimerization and hydrolysis while providing a sustained dose of Paclitaxel with time. Infrared image of the $Apc^{Min/+}$ mouse injected with NPs showed significantly higher concentration of NPs in the intestinal tissue.

KEY WORDS: biodegradable nanoparticle; core-shell morphology; self-assembly; tumor drug delivery.

INTRODUCTION

The American Cancer Society (ACS) estimates that in 2007 about 1.5 million new cases of cancer will be diagnosed in the USA and about 560,000 Americans will die from cancer (1). Although diagnosing cancer at an early stage can significantly improve survival rate, the development of novel technologies that can selectively target and destroy tumor cells, will reduce patient suffering and recovery time. Paclitaxel is a FDA-approved chemotherapeutic drug against a wide spectrum of cancers including ovarian, breast, brain, colon, lung, and AIDS-related cancer (2–4). Short circulation half-life in plasma, limited aqueous solubility, and non-selectivity has limited the use of anti-tumor drugs like Paclitaxel to more invasive and localized methods, like the use of catheters for chemotherapy or surgery to remove the tumor followed by chemotherapy (5–7).

A novel strategy to circumvent the short half-life of the drug, improve patient compliance, and allow targeted delivery to tumor vasculature is to trap the anti-tumor drug in colloidal particles and administer the suspension systemically (8–14). Tumor vasculature presents several abnormalities compared with normal vessels resulting in enhanced permeation and retention effect (EPR effect) (15–17) and NPs with diameter <100 nm are selectively taken up by tumor tissue (18–24). However, the association of cytotoxic drugs with NPs modifies the drug biodistribution profile, because untreated NPs are rapidly opsonized and massively cleared by the fixed macrophages of the mononuclear phagocytes system (MPS) (25, 26). NPs surface modified with hydrophilic polymers like PEG have prolonged half-life in the circulation system, leading to the development of long-circulating, invisible, or stealth NPs for delivery of anti-tumor drugs (27–29). Further-

[1] Biomimetic Materials and Tissue Engineering Laboratories, Department of Chemical Engineering, University of South Carolina, Columbia, South Carolina 29208, USA.
[2] Department of Chemical Engineering, University of South Carolina, Swearingen Engineering Center, Rm 2C11, Columbia, South Carolina 29208, USA.
[3] To whom correspondence should be addressed. (e-mail: jabbari@engr.sc.edu)

more, most tumors lack lymph vessels and higher interstitial fluid pressure than normal tissues, so interstitial fluid and soluble macromolecules are inefficiently removed (30). Therefore, there is accumulation of NPs in the interstitium (EPR effect) which retards their uptake, unless the NPs are degradable (31,32).

Our laboratory has developed novel poly(lactide-co-glycolide-co-fumarate) (PLGF) and poly(lactide-co-ethylene oxide-co-fumarate) (PLEOF) unsaturated macromers that self-assemble to form biodegradable NPs (33–35). The lactide/glycolide units are FDA approved for certain clinical applications, ethylene oxide units are excreted through the kidneys, and fumaric acid units occur naturally in the Kreb's cycle. The degradation characteristics of the NPs can be adjusted by the ratio of lactide to glycolide in the PLGF macromer. The degree of hydrophilicity, hence their circulation half-life, can be controlled by molecular weight and fraction of poly(ethylene glycol) (PEG) in the PLEOF macromer. NPs ranging 50–500 nm in size can be produced by varying the ratio of PLEOF to PLGF in the blend. The unsaturated fumarate groups can be used to covalently attach ligands with high affinity for tumor cells to PLGF/PLEOF NPs.

The objective of this work was to determine tumor cell uptake and cytotoxicity of PLGF/PLEOF and PLAF/PLEOF blend NPs loaded with Paclitaxel. PLGF and PLAF were synthesized by condensation polymerization of ULMW PLGA and ULMW PLA with fumaryl chloride (FuCl). Similarly, PLEOF macromer was synthesized by reacting ULMW PLA and PEG with FuCl. The blend PLGF/PLEOF and PLAF/PLEOF macromers in dimethyl formamide/dimethyl sulfoxide solvent mixture were self-assembled into NPs by dialysis against water. The NPs were characterized with respect to particle size distribution, morphology, and loading efficiency. The physical state and miscibility of Paclitaxel in the NPs were characterized by differential scanning calorimetry (DSC). Tumor cell uptake and cytotoxicity of Paclitaxel loaded NPs were measured by incubation with HCT116 human colon carcinoma cells. The particle uptake was both time and concentration dependent. Results demonstrate that the cytotoxicity of Paclitaxel loaded PLGF/PLEOF NPs incubated with tumor cells is higher than that of Paclitaxel directly added to the culture media.

MATERIALS AND METHODS

Materials

l-Lactide (LA; >99.5% purity) and glycolide (GL; >99.0% purity) monomers were obtained from Ortec (Easley, SC) and Boehringer Chemicals (Ingelheim, Germany), respectively. Dichloromethane (DCM), *N*,*N*-dimethylformamide (DMF), diethyl ether, and hexane were purchased from ACROS (Fairfield, OH). Calcium hydride, Poly(ethylene glycol) (PEG, nominal molecular weights 3.4 kDa), triethylamine (TEA) were purchased from Aldrich (St. Louis, MO). Tin (II) 2-ethylhexanoate (TOC), FITC-dextran (molecular weight 20 kDa; used for imaging NPs, not as a surrogate molecule for release studies), penicillin, streptomycin and tetrazolium dye 3-(4, 5-dimethylthiazol-2-yl)-2, 5-diphenyltetrazolium bromide (MTT) were purchased from Sigma (St. Louis, MO). Fumaryl chloride was obtained from Aldrich and distilled at 161°C prior to use. Diethylene glycol (DEG; >99% purity) was purchased from Fisher (Pittsburgh, PA). Dulbecco's phosphate-buffer saline (PBS), Dulbecco's modified eagle medium (DMEM, high glucose, with L-glutamine, with pyridoxine hydrochloride, without sodium pyruvate), and trypsin-EDTA were purchased from GIBCO BRL (Grand Island, NY). McCoy's culture media was purchased from Mediatech (Herndon, VA). Paclitaxel was obtained from LC Laboratories (Woburn, MA). Spectro/Por dialysis tube (molecular weight cutoff 3.5 kDa) was purchased from Spectrum Laboratories (Rancho Dominquez, CA). Alexa Fluor® 594 Phalloidin and 4,6-diamidino-2-phenylindole (DAPI) were purchased from Molecular Probes (Invitrogen, Carlsbad, CA) and Sigma-Aldrich, respectively. DCM was purified by distillation over calcium hydride. All other solvents were reagent grade and were used as received without further purification.

Macromer Synthesis

ULMW PLA and PLGA were synthesized by ring opening polymerization of L-lactide (LA) and/or Glycolide (GL) monomers with DEG as the initiator and TOC as the polymerization catalyst as described (36–38). LA and GL monomers were dried under vacuum at 40°C for at least 12 h before the reaction. Briefly, 50 g LA and 40 g GL were placed in a three-neck flask, equipped with an overhead stirrer, under a stream of nitrogen. Under constant stirring, temperature was gradually increased to 130°C with an oil bath to melt the monomers. After melting, 5.0 ml of DEG and 5.5 ml of TOC were added to the flask with stirring and reaction was continued for 12 h at 130°C. After the reaction, unreacted monomers and DEG were removed under vacuum (<1 mm Hg) at 140°C for at least 6 h. The product was dissolved in DCM, precipitated in ice-cold ether to remove the high molecular weight fraction. The ether was removed by rotary evaporation and the polymer was re-dissolved in DCM and precipitated twice in hexane. The fractionated ULMW PLA or PLGA was dried under vacuum (<5 mmHg and 40°C) to remove any residual solvent and stored at −20°C. The polymers were characterized by ^{1}H-NMR and gel permeation chromatography (GPC). $\overline{M_n}, \overline{M_w}$, and polydispersity index (PI) of ULMW PLA macromer was 1,450, 1,730 Da, and 1.2, respectively. $\overline{M_n}, \overline{M_w}$, and PI of ULMW PLGA was 1,660, 2,150 Da, and 1.3, respectively. The molecular weight of ULMW PLGA was slightly higher than PLA but they had similar PI values.

In the next step, poly(lactide fumarate) (PLAF) or poly (lactide-co-glycolide fumarate) (PLGF) was synthesized by condensation polymerization of ULMW PLA or PLGA, respectively, with fumaryl chloride (FuCl) as described (36–38). Similarly, for the synthesis of poly(lactide-co-ethylene oxide fumarate) (PLEOF), ULMW PLA and PEG were reacted with FuCl. TEA was used as the acid scavenger. The weight ratio of PLA to PEG was 90:10. The molar ratio of FuCl:(PEG+PLA) and TEA:(PEG+PLA) was 0.9:1.0 and 1.8:1.0, respectively. In a typical reaction, 2.0 g PEG and 18.0 g PLA were dried by azeotropic distillation with toluene and dissolved in 150 ml DCM under dry nitrogen atmosphere in a three-neck reaction flask on ice. After cooling to 5°C, 1.46 ml FuCl and 3.65 ml TEA, each dissolved in 60 ml DCM, were added dropwise to the reaction with stirring. The reaction continued for 6 h on ice followed by 12 h under ambient conditions. After

completion of the reaction, solvent was removed by rotary evaporation and residue was dissolved in 100 ml anhydrous ethyl acetate to precipitate the by-product triethylamine hydrochloride and the salt was removed by filtration. Ethyl acetate was removed by rotary evaporation, the product was dissolved in DCM, and precipitated twice in cold ethyl ether. The polymer was dried in vacuum (<5 mmHg) for at least 12 h and stored at −20°C. PLAF and PLGF macromers were synthesized using a similar procedure. The synthesized PLEOF, PLAF and PLGF macromers were characterized by ^{1}H-NMR and GPC.

Macromer Characterization

The chemical structure of the synthesized macromers was characterized by a Varian Mercury-300 ^{1}H-NMR (Varian, Palo Alto, CA), operated by an O2 workstation (Silicon Graphics, Mountain View, CA), at ambient conditions with 0.17 Hz resolution. The polymer sample was dissolved in deuterated chloroform (Aldrich, 99.8 atom% deuterated) at a concentration of 50 mg/ml and 1% *v/v* trimethylsilane (TMS; Aldrich) was used as the internal standard. The molecular weight distribution of the polymers was measured by GPC (38). Measurements were carried out with a Waters 717 Plus Autosampler GPC system (Waters, Milford, MA) connected to a model 616 HPLC pump, model 600S controller, and a model 410 refractive index detector. The columns consisted of a styragel HT guard column (7.8×300 mm, Waters) in series with a styragel HR 4E column (7.8×300 mm, Waters) heated to 37° C in a column heater. The Empower software (Waters) was used for data analysis and determination of $\overline{M_n}$, $\overline{M_w}$, and PDI. The sample (20 μl), with a concentration of 10 mg/ml in tetrahydrofuran (THF; Sigma-Aldrich), was eluted at a flow rate of 1 ml/min. Monodisperse polystyrene standards (Waters) with peak molecular weights (M_p) ranging from 0.58 to 143.4 kDa and PDI of less than 1.1 were used to construct the calibration curve.

Preparation of Nanoparticles

The PLAF or PLGF macromers and PLEOF in dimethyl formamide/dimethyl sulfoxide (DMF/DMSO) solvent mixture were self-assembled into NPs by dialysis against water (12). For cytotoxicity experiments, self-assembled NPs were prepared with PBS under sterile conditions. Briefly, 45 mg PLAF (or PLGF) and 5 mg PLEOF macromers were dissolved in a solution of 1 ml DMF and 8 ml of DMSO. Next, 3.2 mg Paclitaxel (6% by weight of the macromers) in 1 ml DMSO was added to the macromer solution. The solution was filtered with a 0.2 μm filter (Whatman autovial syringeless filter with a PTFE membrane; Fisher) and loaded in the dialysis tube (molecular cutoff: 3.5 kDa) and dialyzed against sterile phosphate buffer saline (PBS) or distilled deionized water (ddH_2O) under sterile conditions (in a laminar hood). The organic solution was dialyzed against the aqueous phase for 24 h with changes of the dialysis buffer every 4 h until the DMSO and DMF were completely removed. Then, the suspension containing the self-assembled NPs was collected from the dialysis tube and freeze-dried to obtain a free flowing powder. The NPs suspension was used for cytotoxicity experiments without freeze-drying. Drug-free NPs were prepared using a similar procedure without the addition of Paclitaxel. No excipient was used for the preparation and freeze-drying of NPs. However, the PLEOF added to PLAF or PLGF macromer for self-assembly of NPs acted as a stabilizer. The PEG segments of PLEOF stabilize the NPs against aggregation by steric repulsion. The freeze-dried powder was re-suspended in PBS by sonication for 1 min with a 3-mm probe connected to an Ultrasonic Processor (Model CP-130PB-1, continuous mode, Cole-Parmer Instruments, Vernon Hills, IL) with a power and frequency of 10 W and 20 kHz, respectively. After sonication, a noticeable change in particle size distribution of the NPs was not observed before and after freeze-drying, as measured by dynamic light scattering.

Characterization of Nanoparticles

The size distribution of NPs was measured by dynamic light scattering with a NICOMP Submicron Particle Sizer (Autodilute Model 370, NICOMP Particle Sizing Systems, Santa Barbara, CA, USA). Five hundred microliters of the diluted suspension was added to a culture tube and placed in the instrument cell holder. The scattered light intensity was inverted to size distribution by inverse Laplace transform using the CW370 software (NICOMP Particle Sizing Systems). The morphology of the NPs was examined using a JSM-5400 scanning electron microscope (JOEL, Japan) at an accelerating voltage of 20 KeV. Freeze-dried NPs were placed on a graphite surface and coated with gold using an Ion Sputter Coater (JEOL, JFC-1100) at 20 mA for 1 min. The physical state (crystalline *versus* amorphous) and miscibility of Paclitaxel in the NPs were characterized by DSC (Q200, TA instruments, New Castle, DE). 2 mg of the sample, sealed in a DSC aluminum pan, was purged with dry nitrogen at a flow rate of 20 ml/min while the sample was heated from ambient condition to 230°C. The differential heat flow to the sample chamber was measured as a function of temperature. Indium was used as the standard reference material to calibrate the temperature and energy scales of the DSC.

Loading Efficiency

Paclitaxel loaded NPs (6% Paclitaxel by weight of the PLAF or PLGF macromer) were prepared by dialysis as described in section "Preparation of nanoparticles". After dialysis for 24 h to self-assemble the macromers and to remove the unencapsulated Paclitaxel, 2 mg of the NPs were dissolved in 200 μl of DMSO and 3 ml of acetonitrile–water mixture (50:50 *v/v*) was added. After 2 h, the suspension was centrifuged at 15,000 rpm for 10 min and the supernatant was transferred to HPLC (high performance liquid chromatography) vials for determination of Paclitaxel concentration. The drug concentration was determined by isocratic reverse-phase HPLC (Waters system, Milford, MA) using a 250×10 mm, 10 μm Xterra® Prep RP_{18} column (Waters) at a flow rate of 2 ml/min using 50:50 *v/v* acetonitrile/water mixture as the mobile phase. A photodiode array detector (model 996, Waters) was used for detection of Paclitaxel at the wavelength of 227 nm. The elution time of Paclitaxel was 16 min. The measured intensities were correlated to concentrations using a calibration curve constructed with Paclitaxel solutions of known concentration ranging 0.65–65 μg/ml (in the linear range of the detector). The encapsulated amount of Paclitaxel

was divided by the initial amount to determine the encapsulation efficiency.

In Vitro Release Characteristics

The release kinetics of Paclitaxel from the NPs was measured *in vitro* in PBS (pH 7.4) for up to 28 days. Ten milligrams of the Paclitaxel-loaded NPs were suspended in 10 ml of PBS buffer and maintained at 37°C with orbital shaking. At each time point, the suspension was centrifuged at 15,000 rpm for 10 min, and the supernatant was removed and transferred into microvials for HPLC analysis. The precipitate was re-suspended in 10 ml of fresh PBS by sonication for 1 min with a 3-mm probe connected to an Ultrasonic Processor (Cole-Parmer Instruments) with a power and frequency of 10 W and 20 kHz, respectively. The sonicated suspension was maintained in PBS at 37°C with orbital shaking until the next time point. For analysis, the supernatant was first freeze-dried and re-suspended in 1 ml of DMSO to remove the PBS salts. After filtration, DMSO was evaporated and the residual solid was dissolved in 1 ml of 50:50 *v/v* acetonitrile/water mixture for HPLC analysis. The concentration of Paclitaxel in the residual solid was measured with HPLC as described in "Loading efficiency" section.

Cell Culture

HCT116 human colon carcinoma cell line, from America Type Culture Collection (ATCC, Manassas, VA, USA) was obtained from the School of Medicine at University of South Carolina (passages 6–10). HCT116 cell line was cultured in McCoy's Medium supplemented with 10% heat-inactivated fetal bovine serum (FBS; Atlas Biologicals, Fort Collins, CO), 100 U/ml penicillin (Sigma) and 100 μg/ml streptomycin (Sigma) at 37°C in a balanced air humidified incubator with 5% CO_2 and media was changed every 3 days. Cells were rinsed with PBS and enzymatically lifted with 25 μl/cm^2 of 0.05% trypsin (Invitrogen) and 0.53 mM Ethylenediaminetetraacetic acid disodium salt (EDTA; Sigma-Aldrich). Passages 6–10 were used for nanoparticle uptake and cytotoxicity experiments.

Nanoparticle Uptake

HCT116 cells were seeded at a density of 5×10^4 cells/cm^2 on Thermanox plastic coverslips (Nalge Nunc International, Rochester, NY) in 24-well plates and cultured in McCoy's media. Next, the media was replaced with FITC-dextran (10% by weight FITC-dextran in NPs; excitation and emission wavelength of 450/495 and 520 nm) loaded NPs suspension (2 mg/ml) in McCoy's media and the plates were incubated for 2 h. Next, the suspension was removed, wells were washed three times with PBS to remove the remaining NPs, and cells were fixed with 1 ml per well of 4% paraformaldehyde solution in PBS at 37°C for 20 min. After fixation, the paraformaldehyde solution was removed and cells were permeabilized using PBS containing 0.1% Triton X-100 and 100 mM glycine for 30 min and blocked in 1.5% bovine serum albumin/ 0.5% glycine in PBS for 1 h at ambient conditions. For visualization of the cell cytoskeleton, the coverslips were rinsed with PBS and 200 μl of 6.6 μM Alexa Fluor® 594 phalloidin solution (1:200 dilution; excitation and emission wavelength of 581 and 609 nm) was added to each coverslip for 30 min at ambient conditions to stain the actin filaments. Then, coverslips were washed with PBS and the cell nuclei were stained with DAPI (excitation and emission wavelength of 358 and 461 nm) at 1:5,000 dilution. The coverslips were mounted and a confocal scanning laser microscope (Zeiss LSM-510) to take images in the z-plane, perpendicular to the plane of the microscope image. The FITC-dextran loaded nanoparticles were incubated in 1 ml PBS at 37°C for 2 h, the suspension was centrifuged, and the concentration of FITC-dextran in the supernatant was measured by a fluorescent plate reader (Synergy HT, Bio-Tek, Winooski, VT) at excitation and emission wavelength of 495 and 520 nm, respectively. The measured fluorescence was related to FITC-dextran concentration using a calibration curve constructed from fluorescence of solutions with known FITC-dextran concentrations. The released amount of FITC-dextran after 2 h incubation was <2% of the total amount.

Tumor Cell Viability

To measure tumor cell viability, 5×10^4 cells/cm^2 HCT116 tumor cells was seeded per well in 96-well plates and the plates were incubated in McCoy's media for 24 h for cell attachment. Next, the media was changed to McCoy's media containing Paclitaxel, directly added to the media or loaded in NPs, and cells were incubated in that media for 24, 48, and 72 h. The concentration of Paclitaxel in media (loaded in NPs or in solution) was zero, 10, and 40 μg/ml. Since the concentration of Paclitaxel in NPs was 6 wt% (free plus encapsulated), 0.17 and 0.67 mg/ml NPs were added to the media for 10 and 40 μg/ml Paclitaxel, respectively. McCoy's media without NPs was used as the negative control. For direct addition of Paclitxael to McCoy's media, 4 mg Paclitaxel was dissolved in 1 ml DMSO and the solution was diluted 2,000 times by addition of McCoy's media to reach a final concentration of 40 μg/ml. The residual DMSO in the final media was negligible (0.25%) and did not affect the cell viability results. At each time point, the media was removed, wells were washed three times with PBS, and the fraction of viable cells was measured by the MTT assay. In the MTT assay, yellow MTT (3-(4,5-dimethylthiazol-2-yl)-2,5-diphenyltetrazolium bromide) is reduced to purple formazan in the mitochondria of viable cells. 100 μl of the MTT working solution (0.5 mg/ml) was added to each well and incubated at 37°C for 4 h. Next, media was removed, wells were washed with PBS, and 100 μl DMSO was added to solubilize the formazan crystalline product. The absorbance was measured with a plate reader (Synergy HT) at 570 nm and normalized to the absorbance at 630 nm. Fraction of viable HCT116 tumor cells was determined by dividing the normalized absorbance of the test well to that of the control well (without Paclitaxel).

In Vivo Distribution of Nanoparticles

For *in vivo* tracking of NPs, the near-infrared dye IRDye 800RS Carboxylate (LI-COR Biosciences, Lincoln, NE), with peak absorption at 786 nm, was loaded in PLAF/PLEOF NPs under sterile conditions, as described in "Preparation of Nanoparticles". The amount of dye was 2% of the macromer and the concentration of NPs in PBS was 5 mg/ml (100 μg/ml final encapsulated dye concentration). Five hundred microliters of the sterile NPs suspension was injected in the tail vein

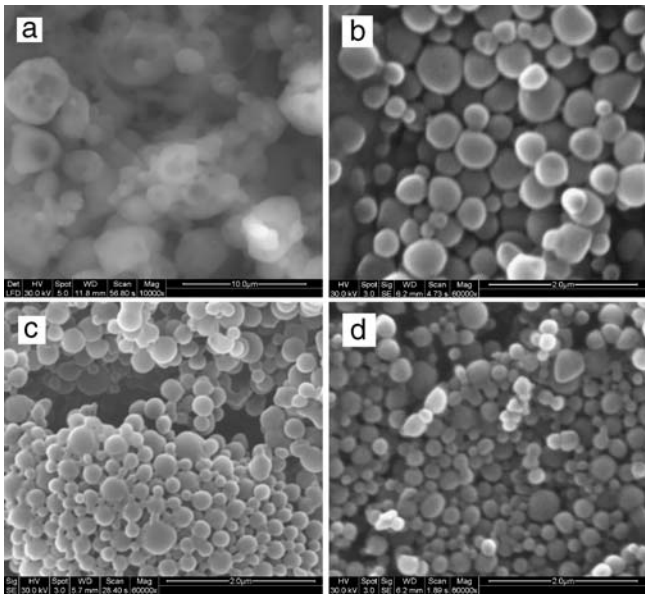

Fig. 1. SEM images of the NPs prepared with PLEOF (**a**), PLGF (**b**), mixture of 90 wt% PLGF and 10% PLEOF (**c**), and mixture of 90% PLGF and 10% PLEOF and loaded with 6 wt% (based on PLGF+ PLEOF weights) Paclitaxel (**d**). The *scale bar* in the images is 2 μm.

of male $APC^{Min/+}$ mice (6 months old; Jackson Laboratories, Bar Harbor, ME). The $Apc^{Min/+}$ mouse has a germline mutation in the adenomatous polyposis coli (Apc) gene, which is responsible for the initiation and development of intestinal tumor [familial adenomatous polyposis; (39)]. The mice were anesthetized with 4.5% isoflurane in an oxygen carrier gas and transferred to the MousePOD™ Adapter (model 9201-MP) scanning surface of an Odyssey Infrared Imaging System (model 9201-3; LI-COR Biosciences). The MousePOD™ adapter was equipped with temperature regulators and nose cones, connected to external source of isoflurane in an oxygen carrier, to maintain animal temperature and the appropriate plane of anesthesia during scanning. The animals were scanned tail to head in two infrared channels simultaneously (700 and 800 nm) where one channel (700 nm channel) was used for normalization of the measured infrared intensities. The intensities were displayed in pseudo colors by the Odyssey software (LI-COR Biosciences) to isolate regions of interest.

RESULTS AND DISCUSSION

Macromer Characterization

$\overline{M_n}, \overline{M_w}$, and PI of the synthesized PLAF was 7.8, 17.4 kDa, and 2.2, respectively; those of PLGF was 9.2 kDa, 19.2, and 2.1; and those of PLEOF was 9.7, 15.4 kDa, and 1.6. The PLAF, PLGF, and PLEOF macromers had similar distributions and molecular weights, although $\overline{M_n}$ of PLAF was slightly lower than PLGF and PLEOF. The PLEOF molecular weight distribution was narrower (PI of 1.6) compared to those of PLAF and PLGF (PI values of >2). The molar ratio of the lactide to glycolide in the macromer can be determined from the area under the peaks in the NMR spectrum centered at 5.21, 4.82, and 1.58 ppm. The lactide/glycolide ratio determined from the NMR spectra was in good agreement with the 50:50 molar ratio in the feed. The presence of a chemical shift with peak location at 6.96 ppm, attributable to hydrogens of the fumarate, confirmed the incorporation of fumarate units in PLGF macromer. The NMR spectrum of PLAF was similar to that of PLGF except the chemical shift centered at 4.82 ppm, due to methylene hydrogens of glycolide, was absent. In the NMR spectrum of PLEOF, the ratio of the peaks due to chemical shifts centered at 5.1 ppm (due to hydrogens attached to the methine group of lactide) and 3.6 ppm (due to methylene hydrogens of the ethylene oxide repeat units) was directly related to the molar ratio of LA to EG monomers in the macromer. Based on NMR results, the PLA to PEG ratio of PLEOF was 6.8. The PLEOF macromer with PLA and PEG molecular weights of 1.4 kDa (PI of 1.2) and 3.4 kDa (PI of 1.1) had $\overline{M_n}$ and PI of 9.7 kDa and 1.58, respectively, as determined by GPC.

Nanoparticle Characterization

Morphology of the NPs, prepared by dialysis, was imaged with SEM. Micrographs a through d in Fig. 1 show the morphology of the NPs prepared with PLEOF, PLGF, 90% PLGF/10% PLEOF, Paclitaxel-loaded 90% PLGF/10% PLEOF macromers, respectively. The PLEOF NPs (Fig. 1a) were relatively large and the spherical shape of the particles eroded upon exposure to the electron beam. Since PLEOF is an amphiphilic macromer (PEG units are hydrophilic while PLA units are hydrophobic), PLEOF NPs had higher water content than PLAF and PLGF. Therefore, after freeze drying, PLEOF NPs had higher porosity compared to PLAF and PLGF NPs. The higher porosity and lower melting temperature (~60°C from rheological experiments) of the PEG segments in PLEOF (compared to that of PLA and PLGA which was >140°) contributed to the instability of the PLEOF NPs under the electron beam. NPs prepared with PLGF macromer (Fig. 1b) were relatively stable under the electron beam (higher melting point of PLGA compared to PEG segments), although some melting and particle–particle bridging were

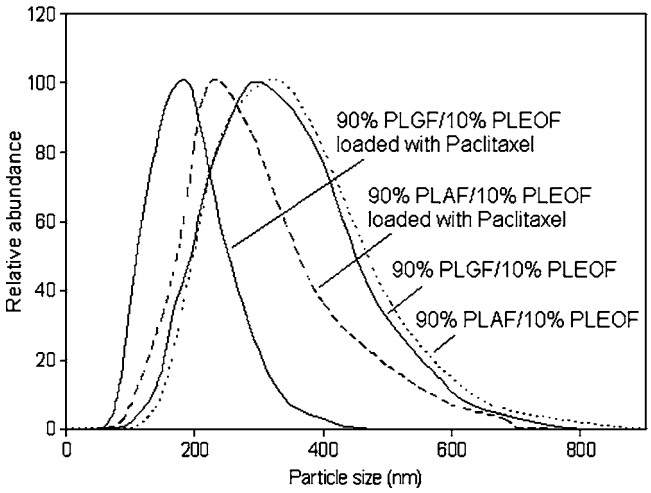

Fig. 2. Size distribution of NPs prepared with PLAF, PLGF, Paclitaxel-loaded 90% PLAF/10%PLEOF, and Paclitaxel-loaded 90% PLGF/10% PLEOF (90:10).

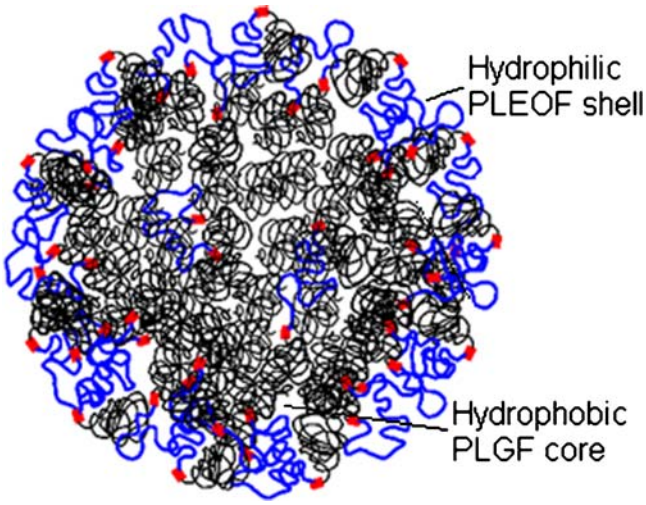

Fig. 3. Schematic diagram of the core-shell structure of PLGF/PLEOF blend NPs.

observed for 90% PLGF/10% PLEOF NPs (Fig. 1c and d). These findings, coupled with smaller particle size and relatively narrow size distribution of NPs prepared with 90% PLGF/10% PLEOF macromers, suggested that the PLEOF macromer was on the surface (not the bulk) of the NPs, functioning as a surface active agent in the process of nanoparticle formation. In the presence of Paclitaxel, the produced PLGF NPs had a narrower particle size distribution and smaller size (see Figs. 1d and 2) compared to those in the absence of Paclitaxel (Fig. 1c). These findings demonstrated that Paclitaxel, with low solubility in aqueous media, acted as seed molecules for self-assembly of PLGF/PLEOF macromers, producing smaller particles with narrower size distribution. The size distribution of NPs was measured by dynamic light scattering and results are shown in Fig. 2. NPs prepared with PLAF and PLGF macromers in the absence of PLEOF and Paclitaxel had average size of 347 and 285 nm, respectively. With the addition of PLEOF macromer (10% by weight of PLAF or PLGF) and Paclitaxel (3 wt%), average size decreased dramatically from 347 to 236 nm for PLAF and from 285 to 190 nm for PLGF. In general, the average size of the NPs prepared with PLAF and PLGF macromers without PLEOF ranged from 250 to 500 nm, while those prepared with PLEOF was 180 to 280 nm.

Based on the results in Figs. 1 and 2, the schematic structure shown in Fig. 3 is contemplated for 90% PLGF/10% PLEOF NPs. The hydrophobic PLAF (PLGF) macromers

Table I. Size of PLAF and PLGF NPs as a Function of Paclitaxel Loading

NPs	PLEOF (%)	Paclitaxel Loading (%)	Mean Size (nm)
PLGF	10	3	190
PLGF	10	6	210
PLGF	10	12	226
PLAF	10	3	236
PLAF	10	6	256
PLAF	10	12	283

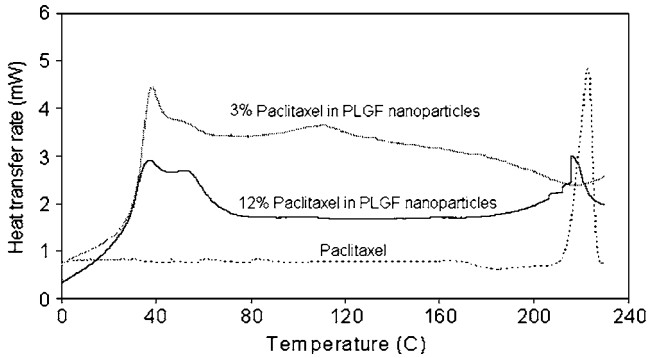

Fig. 4. DSC thermograms of Paclitaxel (*dotted line*), 3 wt% (*solid line*), and 12 wt% (*bold line*) Paclitaxel-loaded PLGF NPs.

occupy the core of the NPs which self-assemble around small seed molecules like Paclitaxel. The PLEOF macromers, due to their amphiphilic character, adsorb on the surface to stabilize the NPs, producing core-shell NPs with PLGF as the core and PLEOF as the shell. The effect of Paclitaxel loading on the size of NPs is summarized in Table I. As the loading was increased from 3 to 6 and 12%, the average size of the NPs prepared with 90% PLGF/10% PLEOF increased from 190 to 210 and 226 nm, respectively, while those prepared with 90% PLAF/10% PLEOF increased from 236 to 256 and 283 nm.

Due to its low aqueous solubility, adjuvants like Cremophor EL are used as solubilizer or emulsifier in Paclitaxel dosage forms. These adjuvants cause serious side effects including hypersensititivity reaction, nephrotoxicity, and neurotoxicity which reduce the drug's therapeutic index and efficacy (6,7,14). Encapsulation of Paclitaxel in degradable and self-stabilizing core-shell PLGF/PLEOF NPs can potentially eliminate the use of adjuvants like Cremophor EL in dosage forms while overcoming the multi-drug resistance in tumor cells (40). Furthermore, degradable self-stabilizing PLEOF shells on PLGF NPs eliminate the need for non-degradable surfactants like poly(vinyl alcohol) that have long circulation time and adversely affect the drug biodistribution and release behavior (41).

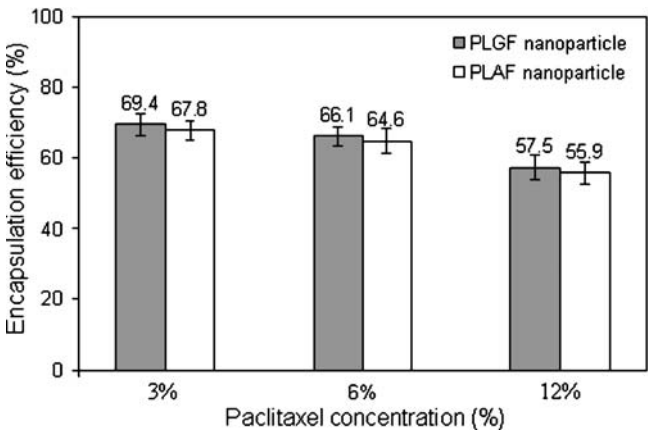

Fig. 5. Encapsulation efficiency of 90% PLAF/10% PLEOF and 90% PLGF/10% PLEOF NPs as a function of Paclitaxel concentration (the values are the mean of four samples with error bars corresponding to one standard deviation from the mean).

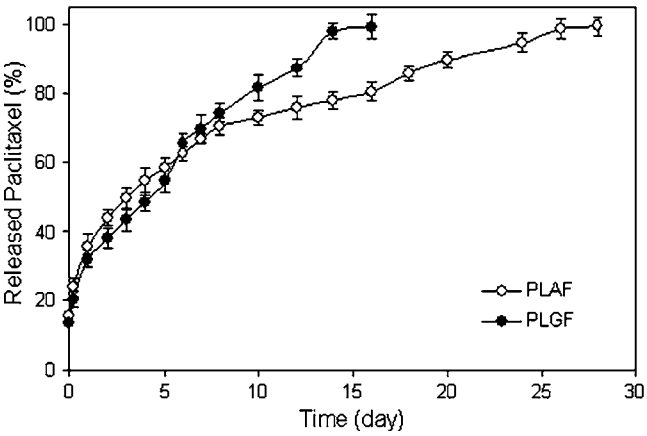

Fig. 6. Cumulative release of Paclitaxel from 90% PLAF/10% PLEOF and 90% PLGF/10% PLEOF NPs as a function of incubation time (the values are the mean of four samples with error bars corresponding to one standard deviation from the mean).

Encapsulation Efficiency and *In Vitro* Release Characteristics

The effect of loading on miscibility and state of Paclitaxel in NPs was investigated with DSC. Fig. 4 compares the DSC thermograms of free Paclitaxel with 3 and 12% Paclitaxel loaded NPs. Free Paclitaxel showed an endothermic melting peak at 223°C. The 3% Paclitaxel loaded PLGF NPs (90% PLGA/10% PLEOF) did not show a melting peak demonstrating that the drug was in a non-crystalline (amorphous) phase or molecularly dissolved in the PLGF matrix. The 12% Paclitaxel loaded NPs showed a sharp melting peak at 223°C indicating that a fraction of Paclitaxel was crystalline and did not dissolve in the PLGF matrix. Therefore, while Paclitaxel in the 3% sample completely dissolved in PLGF, phase separation between Paclitaxel and PLGF occurred for the 12% sample. Our results are consistent with previous findings by Feng *et al.* (42) that phase separation and crystallization of hydrophobic drugs like Paclitaxel can occur in NPs at high drug loading.

The encapsulation efficiency of Paclitaxel in PLAF/PLEOF and PLGF/PLEOF NPs was measured, and the results are shown in Fig. 5. Overall, the encapsulation efficiency ranged from 70 to 56%. The encapsulation efficiency was independent of the macromer (PLAF or PLGF) but it decreased significantly with increasing Paclitaxel loading, consistent with previous results by Xie *et al.* (12). For example, the encapsulation efficiency of PLGF and PLAF for 3% Paclitaxel loading was about 70 and 68%, respectively, while it was 58 and 56% at 12% loading. Since the size of the PLGF NPs (190 nm) was lower than that of PLAF (236 nm; see Table I), particle size did not have a significant effect on encapsulation efficiency in the size range of 100–300 nm.

The release kinetics of Paclitaxel from PLAF and PLGF NPs as a function of incubation time in PBS is shown in Fig. 6. The profiles consisted of a burst release in the first 24 h followed by a period of sustained release. The burst release for PLAF and PLGF NPs loaded with 6% Paclitaxel was 24 and 20%, respectively. The more hydrophobic PLAF NPs released Paclitaxel at a relatively constant rate in 28 days by hydrolytic degradation of the matrix. The less hydrophobic PLGF NPs, due to slight swelling of the matrix, displayed a faster release rate (due to hydrolytic degradation of the slightly swollen matrix). PLGF NPs, due to lower hydrophobicity and faster degradation, released the encapsulated Paclitaxel in 15 days, while PLAF NPs released their content in 28 days. It is noteworthy to mention that no precipitate was obtained for PLAF and PLGF NPs suspensions after 15 and 28 days of incubation, respectively, when suspensions were centrifuged at 15,000 rpm. This indicated that most (if not all) of the PLAF and PLGF NPs degraded after 15 and 28 days, respectively, by hydrolytic degradation and erosion of the matrix. These results demonstrate that there is a mechanistic difference between the release characteristics of PLAF and PLGF NPs and those of high molecular weight (commercially available) PLA and PLGA (43–46). Release of active agents from high molecular weight PLA and PLGA systems is by diffusion through a porous matrix while release from PLAF and PLGF NPs, due to low macromer molecular weight and high density of hydrophilic chain ends, is by hydrolytic degradation and erosion of the matrix (47).

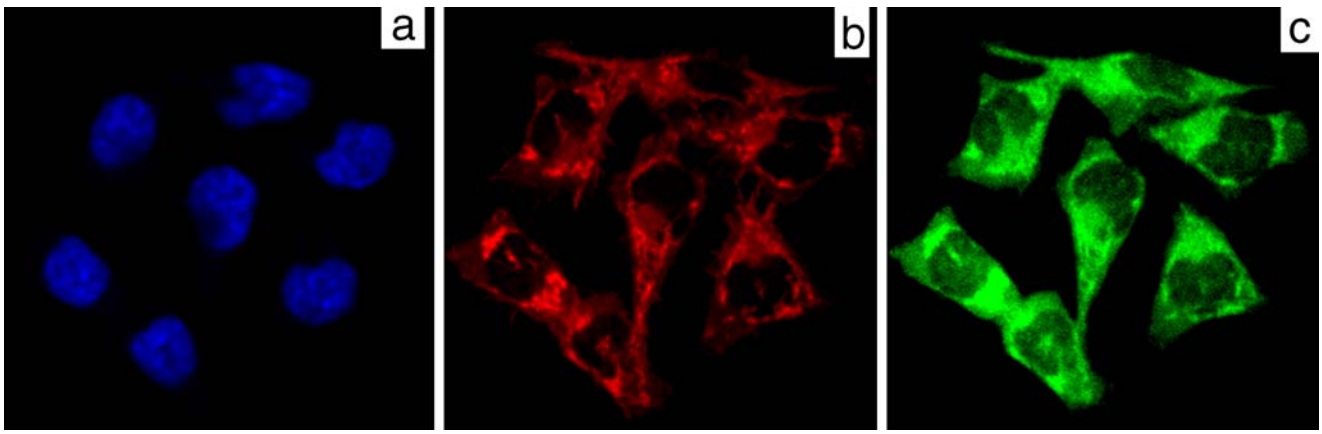

Fig. 7. Confocal fluorescent images of HCT116 tumor cells treated with FITC-dextran loaded PLGF NPs. Micrographs **a**, **b**, and **c** are the images of cell nuclei (DAPI, *blue*), cell cytoskeleton (Alexa Fluor® 594 phalloidin, *red*), and 90% PLGF/10% PLEOF NPs (FITC-dextran, *green*), respectively.

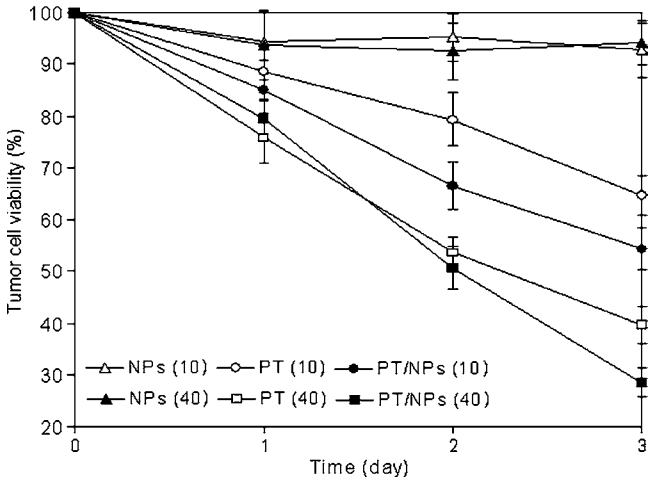

Fig. 8. Viability of HCT116 tumor cells incubated with Paclitaxel in solution or encapsulated in 90% PLAF/10% PLEOF NPs (The values are the mean of four samples with error bars corresponding to one standard deviation from the mean). Experimental groups include empty NPs with amount corresponding to 10 (*open triangles*) and 40 μg/ml (*filled triangles*) Paclitaxel, Paclitaxel in solution with 10 (*open circles*) and 40 μg/ml (*open squares*) concentration, and Paclitaxel loaded in PLGF (90% PLGF/10% PLEOF) NPs with amount corresponding to 10 (*filled circles*) and 40 μg/ml (*filled squares*) Paclitaxel. In the figure legend, "NPs' stands for NPs alone, "PT" stands for Paclitaxel directly added to culture media, and "PT/NPs" stands for Paclitaxel loaded NPs.

Nanoparticle Uptake by Tumor Cells

The uptake of NPs by tumor cells is affected by many factors like particle size and composition, surface polarity and charge, and cell density (48,49). Residual presence of surfactant molecules on the particle's surface can also affect cellular uptake. PLGF nanoparticles (90% PLGF and 10% PLEOF) were loaded with FITC-dextran and their uptake was investigated with HCT116 human colon carcinoma cells by confocal laser scanning microscopy. Fluorescent image of the cell nuclei (DAPI, blue channel), cell cytoskeleton (Alexa Fluor® 594 phalloidin, red channel), and NPs (FITC-dextran, green channel) are shown in Fig. 7a,b, and c, respectively. Comparison of the three images demonstrated that the NPs were internalized by tumor cells (bright spots in the cell cytoplasm in Fig. 7c). Particle uptake can occur either by pinocytosis (a continuous fluid-phase pathway for particles <150 nm) (50) or by phagocytosis (a ligand-induced pathway for particles >200 nm) (51,52). Since size distribution of the particles ranged between 50–350 nm, both pathways contributed to the uptake of NPs. The particle uptake efficiency was both time and concentration dependent (data not shown). As the incubation time was increased from 1 to 4 h, fluorescent intensity of the cell cytoplasm increased, demonstrating that particle uptake was a time-dependent process.

Tumor Cell Viability

To determine cell viability, HCT116 human colon carcinoma cells, seeded in 96 well plates at a density of 5×10^4 cells/cm^2, were incubated in McCoy's media containing Paclitaxel-loaded NPs for up to 3 days. The overall concentration of Paclitaxel was 10 and 40 μg/ml, corresponding to 170 and 670 μg/ml NPs (6 wt% loading) in the media. Cell viability was measured by the MTT assay and results are shown in Fig. 8. Experimental groups included empty NPs with amount corresponding to 10 (open triangles) and 40 μg/ml (filled triangles) Paclitaxel, Paclitaxel in solution with 10 (open circles) and 40 μg/ml (open squares) concentration, and Paclitaxel loaded in PLGF (90% PLGF/10% PLEOF) NPs with amount corresponding to 10 (filled circles) and 40 μg/ml (filled squares) Paclitaxel. The selected concentration range of

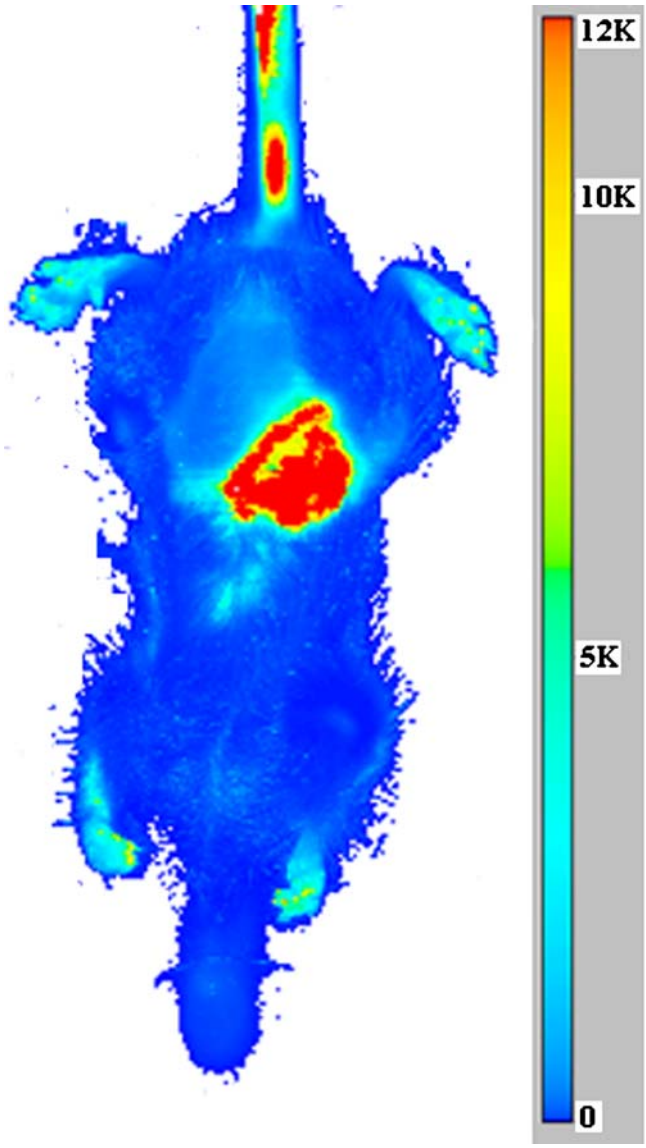

Fig. 9. Near infrared scan (800 nm wavelength) of the Apc$^{Min/+}$ mouse injected with 500 μl of the PLAF/PLEOF NPs encapsulated with the IRDye 800RS Carboxylate dye. The amount of dye was 2% of the macromer and the concentration of NPs in PBS was 5 mg/ml. The NPs suspension was injected in the mouse tail vein and scanned 4 h after injection. 4.5% isoflurane in an oxygen carrier gas was circulated through the nose cone of the MousePOD™ Adapter of the Infrared Imaging System to maintain the appropriate plane of anesthesia during scanning. The intensities are displayed in *pseudo colors* to isolate regions of interest. In the figure *blue color* has a relative infrared intensity of zero while *red* has a relative intensity of 10,000. Since the animal was injected in the tail vein, relatively high NPs concentration is observed in the tail.

Paclitaxel corresponded to the desirable plasma levels of the drug in cancer patients (53). In general, groups with Paclitaxel loaded NPs (with the exception of 40 μg/ml Paclitaxel after 1 day incubation) had lower cell viability compared to Paclitaxel directly added to the media at the same concentration. These results are consistent with previous *in vitro* cytotoxicity results for Paclitaxel (54). As the concentration of Paclitaxel was increased from 0 to 10, and 40 μg/ml, the cell viability of HCT116 cells incubated for three days with free Paclitaxel decreased from 100 to 65 and 40%, respectively, while those encapsulated in PLGF/PLEOF NPs decreased from 93 to 54 and 28%. Since toxicity of Paclitaxel requires entry of the cell in G2 and M cell cycles (55,56), a sustained therapeutic concentration of the drug, rather than a peak plasma concentration, would potentially improve the drug's efficacy, as supported by the results in Fig. 8. The NPs functioned as reservoirs to protect Paclitaxel from epimerization and hydrolysis while providing a sustained dose with time (57). Furthermore, encapsulation in NPs provided other pathways for uptake and intracellular release of the drug. The hydrophobic Paclitaxel in solution is taken up by tumor cells primarily by diffusion through the cell membrane (58,59). On the other side, Paclitaxel loaded NPs attach to tumor cell membrane (although the extent of attachment in the absence of specific ligand-receptor interaction is low), which minimizes the gradient between the extracellular matrix and cell surface, and are internalized by pinocytosis or phagocytosis. Results demonstrate that biodegradable core-shell NPs, with a hydrophobic core and hydrophilic shell, can potentially evade the MPS and overcome resistance at the tumor level as well as increasing cytotoxicity of the anti-tumor drug.

In Vivo Distribution of Nanoparticles

Near-infrared image (800 nm wavelength) of the $Apc^{Min/+}$ mouse injected with 500 μl of the PLAF/PLEOF NPs encapsulated with IRDye 800RS Carboxylate dye (peak absorption at 786 nm) is shown in Fig. 9. The NPs suspension was injected in the mouse tail vein and scanned 4 h after injection. The intensities are displayed in pseudo colors to isolate regions of interest. The infrared intensity in the intestinal region was at least 100 times higher than the other regions. Since the animal was injected in the tail vein, relatively high intensity was observed in the tail, as shown in Fig. 9

CONCLUSIONS

Biodegradable blends of poly(lactide-co-glycolide fumarate) (PLGF) and poly(lactide-co-ethylene oxide fumarate) (PLEOF) macromers were self-assembled into NPs by dialysis. PLEOF macromer, due to its amphiphilic nature, behaved as a surface active agent in the process of self-assembly which produced core-shell NPs with PLGF and PLEOF macromers as the core and shell, respectively. The encapsulation efficiency ranged from 70 to 56% and it was independent of the macromer (PLAF or PLGF) but decreased with increasing concentration of Paclitaxel. PLGF/PLEOF NPs, due to lower hydrophobicity and faster degradation, released Paclitaxel in 15 days, while PLAF/PLEOF NPs released their content in 28 days. The uptake of the NPs by HCT116 human colon carcinoma cells was time-dependent and Paclitaxel loaded NPs had higher cytotoxicity compared to Paclitaxel directly added to the media. The NPs provided other pathways like pinocytosis and phagocytosis for the uptake and intracellular release of Paclitaxel. Near-infrared image of the $Apc^{Min/+}$ mouse injected with 500 μl of the PLAF/PLEOF NPs encapsulated with IRDye 800RS Carboxylate dye showed >100 times higher concentration of NPs in the intestine compared to other tissues. Encapsulation of Paclitaxel in PLGF/PLEOF NPs not only improves cytotoxicity, but it has the potential to evade the mononuclear phagocytes system and target the drug to tumor vasculature.

ACKNOWLEDGEMENTS

This publication was made possible in part by NIH Grant No. P20 RR-016461 from the National Center for Research Resources and by the National Science Foundation/EPSCoR under Grant No. 2001 RII-EPS-0132573. This work was also supported by grants from the AO (Arbeitsgemeinschaft Fur Osteosynthesefragen) Foundation (AORF project 05-J95), and the Aircast Foundation. E. Jabbari thanks Dr. Frank Berger (Center for Colon Cancer Research) at the University of South Carolina for providing the $Apc^{Min/+}$ mouse. E. Jabbari thanks Kelley Intehar (LI-COR Biosciences) for providing the IRDye 800RS Carboxylate dye and scanning the mice with the Odyssey Infrared Imaging System.

REFERENCES

1. ACS. Cancer Facts & Figures. American Cancer Society, Atlanta, GA, Website: http://www.cancer.org/downloads/STT/CAFF2007PWSecured.pdf, (2007).
2. W. P. McGuire, E. K. Rowinsky, N. B. Rosenshein, F. C. Grumbine, D. S. Ettinger, D. K. Armstrong, and R. C. Donehower. Taxol: a unique antineoplastic agent with significant activity in advanced ovarian epithelial neoplasms. *Ann. Intern. Med.* **111**:273 (1989).
3. S. Gagandeep, P. M. Novikoff, M. Ott, and S. Gupta. Paclitaxel shows cytotoxic activity in human hepatocellular carcinoma cell lines. *Cancer Res.* **136**:109 (1999).
4. E. K. Rowinsky, and R. C. Donehower. Paclitaxel (Taxol). *N. Engl. J. Med.* **332**:104 (1995).
5. G. J. MacEachern-Keith, L. J. Wagner, M. J. Butterfield, and I. Mattina. Paclitaxel stability in solution. *Anal. Chem.* **69**:72 (1997).
6. A. K. Singla, A. Garg, and D. Aggarwal. Paclitaxel and its formulations. *Int. J. Pharm.* **235**:179 (2002).
7. H. Gelderblom, J. Verweij, K. Nooter, and A. Sparreboom. Cremophor EL: the drawbacks and advantages of vehicle selection for drug formulation. *Eur. J. Cancer.* **37**:1590 (2001).
8. Q. Zhao, B. Han, Z. Wang, C. Gao, C. Peng, and J. Shen. Hollow chitosan-alginate multilayer microcapsules as drug delivery vehicle: doxorubicin loading and *in vitro* and *in vivo* studies. *Nanomedicine.* **3**:63 (2007).
9. M. Schmitt-Sody, S. Strieth, S. Krasnici, B. Sauer, B. Schulze, M. Teifel, U. Michaelis, K. Naujoks, and M. Dellian. Neovascular targeting therapy: paclitaxel encapsulated in cationic liposomes improves antitumoral efficacy. *Clin. Cancer Res.* **9**:2335 (2003).
10. M. Nahar, T. Dutta, S. Murugesan, A. Senthilkumar, A. Asthana, D. Abhay, D. Mishra, V. Rajkumar, M. Tare, S. Saraf, and N. Kumar. Functional polymeric nanoparticles: an efficient and promising tool for active delivery of bioactives. *Critical Rev. Therap. Drug Carrier Sys.* **23**:259 (2006).
11. T. Ooya, J. Lee, and K. Park. Effects of ethylene glycol-based graft, star-shaped, and dendritic polymers on solubilization and controlled release of paclitaxel. *J. Control. Release.* **93**:121 (2003).

12. J. W. Xie, and C. H. Wang. Self-assembled biodegradable nanoparticles developed by direct dialysis for the delivery of paclitaxe. *Pharm. Res.* **22**:2079 (2005).
13. M. Zeisser-Labouebe, N. Lange, R. Gurny, and F. Delie. Hypericin-loaded nanoparticles for the photodynamic treatment of ovarian cancer. *Int. J. Pharmaceutics.* **326**:174 (2006).
14. C. Fonseca, S. Simoes, and R. Gaspar. Paclitaxel-loaded PLGA nanoparticles: preparation, physicochemical characterization and *in vitro* anti-tumoral activity. *J. Control. Release.* **83**:273 (2002).
15. S. Modi, J. J. Prakash, A. J. Domb, and N. Kumar. Exploiting EPR in polymer drug conjugate delivery for tumor targeting. *Curr. Pharm. Des.* **12**:4785 (2006).
16. A. K. Iyer, G. Khaled, J. Fang, and H. Maeda. Exploiting the enhanced permeability and retention effect for tumor targeting. *Drug Discov. Today.* **11**:812 (2006).
17. L. H. Reddy. Drug delivery to tumours: recent strategies. *J. Pharm. Pharmacol.* **57**:1231 (2005).
18. S. K. Hobbs, W. L. Monsky, F. Yuan, W. G. Roberts, L. Griffith, V. P. Torchilin, and R. K. Jain. Regulation of transport pathways in tumor vessels: role of tumor type and microenvironment. *Proc. Natl. Acad. Sci. U.S.A.* **95**:4607 (1998).
19. S. Unezaki, K. Maruyama, J.-I. Hosoda, I. Nagae, Y. Koyanagi, M. Nakata, O. Ishida, M. Iwatsuru, and S. Tsuchiya. Direct measurement of the extravasation of polyethyleneglycol-coated liposomes into solid tumor tissue by *in vivo* fluorescence microscopy. *Int. J. Pharm.* **144**:11 (1996).
20. O. Gallego, and V. Puntes. Can nanotechnology do to fight cancer? *Clin. Transl. Oncol.* **8**:788 (2006).
21. N. Nishiyama, and K. Kataoka. Current state, achievements, and future prospects of polymeric micelles as nanocarriers for drug and gene delivery. *Pharmacol. Ther.* **112**:630 (2006).
22. C. Vauthier, C. Dubernet, C. Chauvierre, I. Brigger, and P. Couvreur. Drug delivery to resistant tumors: the potential of poly (alkyl cyanoacrylate) nanoparticles. *J. Control. Release* **93**:151 (2003).
23. Y. Kato, H. Onishi, and Y. Machida. Application of chitin and chitosan derivatives in the pharmaceutical field. *Curr. Pharm. Biotechnol.* **4**:303 (2003).
24. I. Brigger, C. Dubernet, and P. Couvreur. Nanoparticles in cancer therapy and diagnosis. *Adv. Drug Deliv. Rev.* **54**:631 (2002).
25. R. M. Owen, C. B. Carlson, J. Xu, P. Mowery, E. Fasella, and L. L. Kiessling. Bifunctional ligands that target cells displaying the $\alpha v\beta 3$ integrin. *ChemBioChem.* **8**:68 (2007).
26. R. Fernandez-Urrusuno, E. Fattal, J. M. Rodrigues, J. Feger, P. Bedossa, and P. Couvreur. Effect of polymeric nanoparticle administration on the clearance activity of the mononuclear phagocyte system in mice. *J. Biomed. Mater. Res.* **31**:401 (1996).
27. M. Cegnar, J. Kristl, and J. Kos. Nanoscale polymer carriers to deliver chemotherapeutic agents to tumours. *Expert Opin. Biol. Ther.* **5**:1557 (2005).
28. S. Kommareddy, S. B. Tiwari, and M. M. Amiji. Long-circulating polymeric nanovectors for tumor-selective gene delivery. *Technol. Cancer Res. Treat.* **4**:615 (2005).
29. G. Kaul, and M. Amiji. Biodistribution and targeting potential of poly(ethylene glycol)-modified gelatin nanoparticles in subcutaneous murine tumor model. *J. Drug Target.* **12**:585 (2004).
30. C.-H. Heldin, K. Rubin, K. Pietras, and A. Ostman. High interstitial pressure- An obstacle in cancer therapy. *Nature Rev.* **4**:806 (2004).
31. H. Maeda, J. Fang, T. Inutsuka, and Y. Kitamoto. Vascular permeability enhancement in solid tumor: various factors, mechanisms involved and its implications. *Int. Immunopharmacol.* **3**:319 (2003).
32. S. N. Ettinger, C. C. Poellmann, N. A. Wisniewski, A. A. Gaskin, J. S. Shoemaker, J. M. Poulson, M. W. Dewhirst, and B. Klitzman. Urea as a recovery marker for quantitative assessment of tumor interstitial solutes with microdialysis. *Cancer Res.* **61**:7964 (2001).
33. E. Jababri, and X. He. Release characteristics of novel bioresorbable *in-situ* crosslinkable self-assembled nanoparticles. *CRS Abstract.* **CS**:1 (2007).
34. E. Jabbari, and X. He. Synthesis and characterization of bioresorbable *in situ* crosslinkable ultra low molecular weight poly(lactide) macromer. *J. Mater. Sci. Mater. Med.* **PMID**:17597374 (2007).
35. X. He, and E. Jabbari. Material properties and cytocompatibility of injectable MMP degradable poly(lactide ethylene oxide fumarate) hydrogel as a carrier for marrow stromal cells. *Biomacromolecules.* **8**:780 (2007).
36. A. S. Sarvestani, X. He, and E. Jabbari. The Effect of osteonectin-derived peptide on the viscoelasticity of hydrogel/apatite nanocomposite scaffolds. *Biopolymers.* **85**:370 (2007).
37. E. Jabbari, and X. He. Synthesis and material properties of functionalized lactide oligomers as *in situ* crosslinkable scaffolds for tissue regeneration. *Polym. Prepr.* **47**:353 (2006).
38. A. S. Sarvestani, X. He, and E. Jabbari. Rheological characterization and modeling of gelation kinetics of injectable *in situ* crosslinkable poly (lactide-ethylene oxide-fumarate) hydrogels. *Biomacromolecules.* **8**:406 (2007).
39. J. Groden, A. Thliveris, W. Samowitz, M. Carlson, L. Gelbert, H. Albertsen, G. Joslyn, J. Stevens, L. Spirio, and M. Robertson. Identification and characterization of the familial adenomatous polyposis coli gene. *Cell.* **66**:589 (1991).
40. A. Sparreboom, J. van Asperen, U. Mayer, A. H. Schinkel, J. W. Smit, D. K. Meijer, P. Borst, W. J. Nooijen, J. H. Beijnen, and O. van Tellingen. Limited oral bioavailability and active epithelial excretion of paclitaxel (Taxol) caused by P-glycoprotein in the intestine. *Proc. Natl. Acad. Sci. USA* **94**:2031 (1997).
41. P. D. Scholes, A. G. Coombes, L. Illum, S. S. Davis, J. F. Watts, C. Ustariz, M. Vert, and M. C. Davies. Detection and determination of surface levels of poloxamer and PVA surfactant on biodegradable nanospheres using SSIMS and XPS. *J. Control. Release.* **59**:261 (1999).
42. L. Mu, and S. S. Feng. PLGA/TPGS nanoparticles for controlled release of paclitaxel: effects of the emulsifier and drug loading ratio. *Pharm. Res.* **20**:1864 (2003).
43. H. B. Ravivarapu, H. Lee, and P. P. DeLuca. Enhancing initial release of peptide from poly(d,llactide-co-glycolide) (PLGA) microspheres by addition of a porosigen and increasing drug load. *Pharm. Dev. Technol.* **5**:287 (2000).
44. A. Messaritaki, S. J. Black, C. F. van der Walle, and S. P. Rigby. NMR and confocal microscopy studies of the mechanisms of burst drug release from PLGA microspheres. *J. Control. Release.* **108**:271 (2005).
45. J. Siepmann, K. Elkharraz, F. Siepmann, and D. Klose. How autocatalysis accelerates drug release from PLGA-based microparticles: a quantitative treatment. *Biomacromolecules.* **6**:2312 (2005).
46. D. Klose, F. Siepmann, K. Elkharraz, S. Krenzlin, and J. Siepmann. How porosity and size affect the drug release mechanisms from PLGA-based microparticles. *Int. J. Pharm.* **314**:198 (2006).
47. E. Jabbari, W. Xu, and X. He. Degradation characteristics of novel *in-situ* crosslinkable poly(lactide-co-glycolide-ethylene oxide-fumarate) copolymer networks. *Trans. Soc. Biomaterials.* **1**:353 (2007).
48. M. O. Oyewumi, R. A. Yokel, M. Jay, T. Coakley, and R. J. Mumper. Comparison of cell uptake, biodistribution and tumor retention of folate-coated and PEG-coated gadolinium nanoparticles in tumor-bearing mice. *J. Control. Release.* **95**:613 (2004).
49. M. O. Oyewumi, and R. J. Mumper. Influence of formulation parameters on gadolinium entrapment and tumor cell uptake using folate-coated nanoparticles. *Int. J. Pharm.* **251**:85 (2003).
50. M. Louis, D. Beck, D. Merkle, and G. Ciraolo. Particle size does not affect the rate of intracellular routing for ligands internalized by non-adsorptive pinocytosis. *J. Electron Microsc.* **46**:337 (1997).
51. B. D. Chithrani, A. A. Ghazani, and W. C. Chan. Determining the size and shape dependence of gold nanoparticle uptake into mammalian cells. *Nano Lett.* **6**:662 (2006).
52. H. L. Wong, R. Bendayan, A. M. Rauth, H. Y. Xue, K. Babakhanian, and X. Y. Wu. A mechanistic study of enhanced doxorubicin uptake and retention in multidrug resistant breast cancer cells using a polymer-lipid hybrid nanoparticle system. *J. Pharmacol. Exp. Ther.* **317**:1372 (2006).
53. Taxol clinical pharmacology, RxList. http://www.rxlist.com/cgi/generic/paclitaxel_cp.htm.
54. I. Gut, V. Danielova, J. Holubova, P. Soucek, and H. Kluckova. Cytotoxicity of cyclophosphamide, paclitaxel, and docetaxel for tumor cell lines *in vitro*: effects of concentration, time and cytochrome P450-catalyzed metabolism. *Arch. Toxicol.* **74**:437 (2000).

55. C. H. Shu, W. K. Yang, Y. L. Shih, M. L. Kuo, and T. S. Huang. Cell cycle G2/M arrest and activation of cyclin-dependent kinases associated with low-dose paclitaxel-induced sub-G1 apoptosis. *Apoptosis.* **2**:463 (1997).
56. T. H. Wang, H. S. Wang, and Y. K. Soong. Paclitaxel-induced cell death: where the cell cycle and apoptosis come together. *Cancer.* **88**:2619 (2000).
57. W. P. McGuire. Paclitaxel in cancer treatment. Informa Health Care, Oxon, UK, 1995, p. 7.
58. M. G. Catalano, L. Costantino, N. Fortunati, O. Bosco, M. Pugliese, G. Boccuzzi, L. Berta, and R. Frairia. High energy shock waves activate 5'-aminolevulinic acid and increase permeability to Paclitaxel: antitumor effects of a new combined treatment on anaplastic thyroid cancer cells. *Thyroid.* **17**:91 (2007).
59. M. V. Varma, and R. Panchagnula. Enhanced oral paclitaxel absorption with vitamin E-TPGS: effect on solubility and permeability *in vitro*, *in situ* and *in vivo*. *Eur. J. Pharm. Sci.* **25**:445 (2005).